American Mineralogist, Volume 88, pages 1115–1128, 2003

Coupling between non-convergent ordering and transition temperature in the $C2/c \leftrightarrow P2_1/c$ phase transition in pigeonite

FERNANDO CAMARA,[1,*] MICHAEL A. CARPENTER,[2] M. CHIARA DOMENEGHETTI,[3] AND VITTORIO TAZZOLI[3]

[1]CNR-Istituto di Geoscienze e Georisorse, sezione di Pavia, via Ferrata 1, I-27100 Pavia, Italy
[2]Department of Earth Sciences, University of Cambridge, Downing Street, Cambridge CB2 3EQ, U.K.
[3]Dipartimento Scienze della Terra, Università di Pavia, Via Ferrata 1, I-27100 Pavia, Italy

ABSTRACT

A Landau potential with linear-quadratic coupling has been developed to describe interactions between a non-convergent order parameter, Q_{OD}, for Fe/Mg ordering, and the order parameter, Q_D, for the $C2/c$-$P2_1/c$ phase transition in pigeonite. Spontaneous strain relationships, and expressions for the effect of ordering on the transition temperature derived from this expansion, have been tested by single crystal X-ray diffraction methods. Lattice parameters collected from a natural pigeonite crystal with composition $En_{47}Fs_{44}Wo_9$, in situ at temperatures up to 1050 °C, reveal that increasing Q_{OD} could act to suppress Q_D by a mechanism which includes overlapping and opposing strain fields. In a second experiment, the intensities of superlattice reflections ($h + k = 2n + 1$) were followed in situ at temperatures up to 500 °C. The crystal was heated ex situ successively at 700, 750, 800, and 850 °C between repeated in situ measurements in order to produce changes in the degree of cation order. The resulting data sets, giving the temperature dependence of Q_D^2 for different fixed values of Q_{OD}, are consistent with the initial Landau model. In particular, they show a strong and linear dependence of transition temperature on Q_{OD}. The fourth order coefficient of the expansion describing the phase transition is perhaps also renormalized by changes in Q_{OD}. It is suggested that the influence of Q_{OD} on the phase transition could be greater than the influence of the phase transition on the equilibrium variation of Q_{OD}.

INTRODUCTION

Pigeonite $(Mg,Fe^{2+},Ca)(Mg,Fe^{2+})(Si_2O_6)$ has space group $P2_1/c$ at room temperature. This structure contains two symmetrically distinct chains of SiO_4 tetrahedra. At high temperatures it has space group $C2/c$, and previous studies have shown that a $C2/c$-$P2_1/c$ transition occurs by rotations of the tetrahedra until the two chains become symmetrically equivalent (Brown et al. 1972; Smyth 1974; Pannhorst 1984; Schröpfer 1985; Arlt et al. 2000). The thermodynamic character of the transition varies with composition. Smyth (1974) and Tribaudino et al. (2002) reported first order character for crystals with composition $En_{32}Fs_{66}Wo_2$ and $En_{92}Wo_8$, respectively. By way of contrast, Cámara et al. (2002) found that the transition is second order in crystals with composition $En_{47}Fs_{43}Wo_{10}$. The same phase transition in natural kanoite ($MnMgSi_2O_6$) is first order (Arlt and Armbruster 1997), in synthetic ferrian magnesian spodumene it is tricritical (Cámara et al. 2003), and in synthetic $LiFeSi_2O_6$ it is close to tricritical (Zhang et al. 2002). Data in the literature show that the transition temperature decreases with increasing Fe^{2+}-content and Ca^{2+}-content in the Ca,Mg,Fe pigeonite solid solution (Prewitt et al. 1971; Tribaudino 2000), and with increasing Na^+-content in natural kanoite crystals (Arlt et al. 2000).

Octahedrally coordinated cations (mainly Fe^{2+} and Mg) in pigeonite crystals are distributed between M1 and M2 sites in a strongly temperature dependent manner (Woodland et al. 1997; Angel et al. 1998; Pasqual et al. 2000; Cámara et al. 2002). Calcium, due to its large ionic radius, is considered to be fully ordered at the larger M2 site. Cámara et al. (2002) have shown that the $C2/c$-$P2_1/c$ transition is influenced by this non-convergent ordering as well as by composition. The simplest explanation for such a dependence is that increasing Fe/Mg disorder causes the average size of cations at the M2 site to decrease, which, in turn, destabilizes the $C2/c$ structure with respect to the $P2_1/c$ structure and transition temperature increases. It follows that, under equilibrium conditions, there is a complex relationship between the displacive order parameter, Q_D, and the non-convergent order parameter, Q_{OD}. Q_{OD} will change as a consequence of the displacive transition and the displacive transition temperature will change as a function of Q_{OD}. These interdependencies can be described qualitatively in terms of the size of the M2 site, or some other crystallographic parameter, but a quantitative analysis requires a more formal definition of the coupling between the two order parameters.

Following on from the work described in Cámara et al. (2002), the main objectives of this paper are (1) to present formal Landau theory which describes the effects of coupling between a non-convergent order parameter (Q_{OD}) and a symmetry breaking order parameter (Q_D), and (2) to demonstrate how this leads to a simple relationship between the displacive transition temperature and the degree of non-convergent Fe/Mg order

* E-mail: camara@crystal.unipv.it

which can be tested experimentally. The proposed coupling model is based on interactions between competing strain effects, so the lattice parameter changes due to the phase transition and to cation ordering are also analyzed formally in terms of spontaneous strains. The results are applicable generally to systems in which order parameter coupling is linear-quadratic in character, but they are used here to analyze experimental data for a single crystal of pigeonite which has been heat treated to induce different degrees of order. Data from in situ measurements of the intensities of superlattice reflections also suggest that the thermodynamic character of the transition could be modified by changes in Fe/Mg order.

LANDAU THEORY FOR A SYSTEM WITH LINEAR-QUADRATIC COUPLING BETWEEN TWO ORDER PARAMETERS

Q_D is a symmetry breaking order parameter which transforms as the active representation for the $C2/c$-$P2_1/c$ transition. Q_{OD} is non-symmetry breaking, in the sense that it describes Fe/Mg ordering which does not lead to a phase transition. It transforms as the identity representation of space group $C2/c$. The lowest order coupling between the two order parameters that is permitted by symmetry has the form $\lambda Q_{OD}Q_D^2$, where λ is a coupling coefficient. The physical origin of this coupling can probably be understood at a macroscopic level in terms of common strain effects, as discussed by Salje (1985) and Salje et al. (1985) for bilinear coupling in albite. Changes in both Q_D and Q_{OD} should induce some lattice strain. The strain due to Q_{OD} will interact with the strain due to Q_D so that a change in Q_{OD} indirectly causes a change in Q_D, and vice versa. Adopting the approach pioneered by Salje (1985) and set out for linear-quadratic coupling by Carpenter (1992), a single Landau expansion in two order parameters with separate coupling to a generalized strain is

$$\begin{aligned} G = {} & -hQ_{OD} + \frac{1}{2}a_{OD}(T - T_{cOD})Q_{OD}^2 + \frac{1}{n}e_{OD}Q_{OD}^n \\ & + \frac{1}{2}a_D(T - T_{cD})Q_D^2 + \frac{1}{4}b_DQ_D^4 + \frac{1}{6}c_DQ_D^6 + d_{OD}\varepsilon Q_{OD} + d_D\varepsilon Q_D^2 + f\varepsilon^2 \\ & + n_{OD}XQ_{OD} + o_{OD}XQ_{OD}^2 + n_DXQ_D^2 + o_DXQ_D^4. \end{aligned} \quad (1)$$

Here h is the field term for non-convergent ordering, which determines that complete disorder ($Q_{OD} = 0$) does not occur at any finite temperature (Salje and Kroll 1991; Carpenter et al. 1994); $a - e$ are Landau coefficients, f is a combination of elastic constants, and ε represents the strain. A single term in Q_{OD}^n is used to represent the combined contributions of all higher order terms in the expansion for non-convergent ordering; convenient values of n are 4 or 6 (Carpenter et al. 1994). The effects of composition are expressed in terms of separate coupling between each order parameter and a compositional parameter, X. These coupling terms are given to second order in Q_{OD} and fourth order in Q_D, with coefficients n_D, n_{OD}, and o_D, o_{OD}. X represents Fe/Mg-content or Ca-content, which could also be incorporated separately using different coupling coefficients.

At equilibrium, the excess free energy must be at a minimum with respect to strain, giving

$$\begin{aligned} & \frac{\partial G}{\partial \varepsilon} = 0 = d_{OD}Q_{OD} + d_DQ_D^2 + 2f\varepsilon \\ & \Rightarrow \varepsilon = -\left(\frac{d_{OD}Q_{OD} + d_DQ_D^2}{2f}\right). \end{aligned} \quad (2)$$

Substituting back into Equation 1 and grouping terms differently gives

$$\begin{aligned} G = {} & (-h + n_{OD}X)Q_{OD} + \frac{1}{2}a_{OD}\left(T - T_{cOD} - \frac{d_{OD}^2}{2a_{OD}f} + \frac{2o_{OD}X}{a_{OD}}\right)Q_{OD}^2 + \frac{1}{n}e_{OD}Q_{OD}^n \\ & + \frac{1}{2}a_D\left(T - T_{cD} + \frac{2n_D}{a_D}X\right)Q_D^2 + \frac{1}{4}\left(b_D - \frac{d_D^2}{f} + 4o_DX\right)Q_D^4 + \frac{1}{6}c_DQ_D^6 \\ & - \frac{d_Dd_{OD}}{2f}Q_{OD}Q_D^2. \end{aligned} \quad (3)$$

The critical temperatures are again normalized to

$$T_{cOD}^* = T_{cOD} + \frac{d_{OD}^2}{2a_{OD}f} - \frac{2o_{OD}X}{a_{OD}} \quad (4)$$

$$T_{cD}^* = T_{cD} - \frac{2n_D}{a_D}X, \quad (5)$$

and the fourth order coefficient for the displacive order parameter is renormalized to

$$b_D^* = b_D - \frac{d_D^2}{f} + 4o_DX. \quad (6)$$

The coefficient in the linear-quadratic coupling term can be replaced by

$$\lambda = \frac{d_Dd_{OD}}{2f}. \quad (7)$$

Finally, if all the terms in Q_D^2 are grouped, including linear-quadratic coupling, the transition temperature of the $C2/c$-$P2_1/c$ transition becomes

$$T_{cD}^{**} = T_{cD} - \frac{2n_D}{a_D}X + \frac{2\lambda}{a_D}Q_{OD}. \quad (8)$$

The conditions for equilibrium derived from Equation 3 are

$$\frac{\partial G}{\partial Q_{OD}} = 0 = -h + a_{OD}(T - T_{cOD}^*)Q_{OD} + e_{OD}Q_{OD}^{n-1} - \lambda Q_D^2 \quad (9)$$

$$\frac{\partial G}{\partial Q_D} = 0 = a_D(T - T_{cD}^*) + b_D^*Q_D^2 + c_DQ_D^4 - 2\lambda Q_{OD}. \quad (10)$$

The evolution of Q_D and Q_{OD} with temperature must be consistent with both these constraints but, because Fe/Mg ordering is kinetically hindered at low temperatures, it is possible to explore the relationships in Equation 10 by observing the variation of Q_D as a function of temperature in crystals with a fixed composition and with different fixed values of Q_{OD}. The expression which can be tested experimentally in this context is

$$T = T_{cD}^{**} - \frac{b_D^*}{a_D}Q_D^2 - \frac{c_D}{a_D}Q_D^4, \quad (11)$$

with

$$T_{cD}^{**} = T_{cD}^* + \frac{2\lambda}{a_D}Q_{OD}. \quad (12)$$

The conventional definition for an order parameter to describe distributions of equal numbers of Fe and Mg atoms between two sites, M1 and M2, would be

$$Q_{OD} = \frac{X_{Fe}^{M2} - X_{Fe}^{M1}}{X_{Fe}^{M2} + X_{Fe}^{M1}}, \quad (13)$$

where X_{Fe}^{M2} and X_{Fe}^{M1} are the average occupancies by Fe atoms of the M2 and M1 sites, respectively. This order parameter scales between 0 for complete disorder and 1 for complete order, in the usual way. If the Fe:Mg ratio is not 1:1, as at Mg-rich or Fe-rich compositions in a solid solution between $Mg_2Si_2O_6$ and $Fe_2Si_2O_6$, this definition gives $Q_{OD} = 1$ for maximum order at Mg-rich compositions but $Q_{OD} < 1$ for maximum order at Fe-rich compositions. To obtain $Q_{OD} = 1$ for complete order in the Fe-rich end of the solid solution, it is necessary to express Q_{OD} as

$$Q_{OD} = \frac{X_{Mg}^{M1} - X_{Mg}^{M2}}{X_{Mg}^{M1} + X_{Mg}^{M2}}. \quad (14)$$

Alternatively, the definition used by Carpenter and Salje (1994), $Q_{OD} = X_{Fe}^{M2} - X_{Fe}^{M1}$, can be used, with the value of Q_{OD} referring to complete order only at the 1:1 composition. When there is calcium present, it is necessary to take account of the fact that the M2 site is partially occupied by atoms which do not participate in the order/disorder process. In order to constrain the value of $Q_{OD} = 0$ to represent maximum Fe/Mg disorder between the M1 and M2 sites, X_{Fe}^{M2} and X_{Fe}^{M1} may be defined as

$$X_{Fe}^{M1} = \left[\frac{Fe^{M1} + Mn^{M1}}{Fe^{M1} + Mn^{M1} + Mg^{M1}} \right] \quad (15)$$

and

$$X_{Fe}^{M2} = \left[\frac{Fe^{M2} + Mn^{M2}}{Fe^{M2} + Mn^{M2} + Mg^{M2}} \right], \quad (16)$$

rather than as the average occupancy of each site by Fe (+Mn). Equivalent expressions for Mg are

$$X_{Mg}^{M1} = \left[\frac{Mg^{M1}}{Fe^{M1} + Mn^{M1} + Mg^{M1}} \right] \quad (17)$$

and

$$X_{Mg}^{M2} = \left[\frac{Mg^{M2}}{Fe^{M2} + Mn^{M2} + Mg^{M2}} \right]. \quad (18)$$

Assuming that calcium is located exclusively at the M2 site, the sum $Fe^{M2} + Mn^{M2} + Mg^{M2}$ will be correspondingly less than 1. The equilibrium partition coefficient, K_D, is still given by

$$K_D = \frac{X_{Fe}^{M1} . X_{Mg}^{M2}}{X_{Fe}^{M2} . X_{Mg}^{M1}}, \quad (19)$$

when Ca is present at M2, if X_{Fe}^{M2}, X_{Fe}^{M1}, etc., are as specified by Equations 15–18.

Spontaneous strains accompanying both the $C2/c$-$P2_1/c$ transition and cation ordering in pigeonite are given by (from Carpenter et al. 1998)

$$e_{11} = \frac{a}{a_o} - 1 \quad (20)$$

$$e_{22} = \frac{b}{b_o} - 1 \quad (21)$$

$$e_{33} = \frac{c \sin\beta}{c_o \cos\beta_o} - 1 \quad (22)$$

$$e_{12} = e_{23} = e_{21} = e_{32} = 0 \quad (23)$$

$$e_{13} = e_{31} = \frac{1}{2}\left(\frac{c \cos\beta}{c_o \sin\beta_o} - \frac{a \cos\beta_o}{c_o \sin\beta_o} \right). \quad (24)$$

The reference parameters, a_o, b_o, c_o, β_o, all refer to structural states with $Q_D = 0$ for strains coupled to Q_D and with $Q_{OD} = 0$ for strains coupled to Q_{OD}. The volume strain V_s is given by

$$V_s = \frac{V}{V_o} - 1. \quad (25)$$

As discussed above for coupling with the generalized strain, ε, coupling between individual strain components and the two order parameters is expected to be of the form $\lambda e_{ik} Q_{OD}$ and $\lambda e_{ik} Q_D^2$, with i,k = 1-3.

SAMPLES

Two single crystals of volcanic pigeonite extracted from sample BTS-308, a rhyodacite from Paraná (Brazil), were used for the experiments. Their composition, $En_{47}Fs_{44}Wo_9$, is nearly the same as crystal BTS-308 no. 2 previously studied by Pasqual et al. (2000) ($\sim En_{47}Fs_{43}Wo_{10}$). The pigeonite crystals in sample BTS-308 are exsolution free, as described by Pasqual et al. (2000) after TEM observations. The absence of augite exsolution was also checked by analyzing diffraction rocking profiles on a single crystal diffractometer.

METHODOLOGY AND EXPERIMENTAL DATA

Ex situ annealing experiments

Crystal BTS-308 no. 17 was heated successively at 700, 750, 800, and 850 °C in order to induce the equilibrium degrees of Fe/Mg intracrystalline order corresponding to each of these temperatures. The annealing was done in a vertical furnace following the procedure described by Zema et al. (1997), for times that are listed in Table 1. Before any heat treatment and after ex situ annealing, the degree of Fe/Mg order was measured by complete X-ray data collection and refinement. Annealing temperatures and times are reported in Table 1. The equilibration temperature for the natural sample has been calculated as 636 °C using the refined degree of order and the $\ln K_D$ vs. ($1/T$) calibration of Pasqual et al. (2000).

In-situ heating experiments

Prior to ex situ heat treatment, crystal BTS-308 no. 17 was heated in situ using a horseshoe resistance heater fitted to the Philips PW1100 automated four-circle diffractometer at CNR-IGG. This furnace allows temperatures up to 1100 °C to be achieved and intensity data in the 2θ range 3-58° to be collected. It has been calibrated for temperature using the melting points of selected standards (Tribaudino et al. 2002). Temperature at the crystal varies by ± ~10 °C depending on the orientation of the heater during data collection. Crystal no. 17 was held in a sealed quartz vial (1 mm Ø) together with some graphite powder to prevent oxidation of Fe^{2+} to Fe^{3+}. To avoid any mechanical stress, it was kept in position within the vial using quartz wool. Starting from room temperature, lattice parameters were measured by centering 24 selected hkl a-reflections ($h + k = 2n$). After this, the intensities of b-reflections ($h + k = 2n + 1$: 102, 052, $\bar{7}02$, $\bar{2}\bar{3}3$, $\bar{2}33$) were determined by measuring step scan profiles of 3° by ω-rotations. For scaling purposes, the intensities of adjacent a-reflections in the same reciprocal row (202, 062, $\bar{6}02$, $\bar{1}\bar{3}3$, $\bar{1}33$) were also measured. The crystal was heated at temperatures up to 500 °C in steps of 25 °C. At each temperature, the

TABLE 1. Details of annealing experiments on crystal BTS-308 n.17

Sample	Treatment		Buffer in-situ	Buffer ex-situ
	in-situ	ex-situ		
BTS-308 n.17_1	up to 500°C		powdered graphite	
BTS-308 n.17_2	up to 500°C	at 700°C for 192 hours	powdered graphite	Fe-wustite
BTS-308 n.17_3	up to 500°C	at 750°C for 120 hours	powdered graphite	Fe-wustite
BTS-308 n.17_4	up to 500°C	at 800°C for 117 hours	powdered graphite	Fe-wustite
BTS-308 n.17_5	up to 500°C	at 850°C for 6 hours	powdered graphite	Fe-wustite
BTS-308 n.17_6			powdered graphite	

intensity and lattice parameter measurements were repeated. The maximum temperature of 500 °C was imposed so as to prevent any change in the degree of Fe/Mg order during the in situ measurements. The same crystal was then heated at 700 °C, ex situ, as described above, before being remounted for a further set of in situ measurements up to 500 °C. The same procedure was repeated after each of the ex situ heat treatments listed in Table 1. A complete data collection and refinement, following the complete sequence, confirmed that no reordering could have taken place at temperatures below 500 °C during the in situ experiments. All the data for the intensities of b-reflections (summed as ΣI_b) and of the a-reflections (summed as ΣI_a) are given in Table 2 as the ratio $\Sigma I_b/\Sigma I_a$. Lattice parameter data are given in Table 3.

Crystal BTS-308 no. 14 was also mounted in a sealed quartz vial, as described above. It was not subjected to any ex situ heat treatments but, instead, was heated in situ at a succession of temperatures from room temperature up to 1050 °C. At each temperature, the intensities of a- and b-reflections were measured and data were collected for lattice parameter refinements. These measurements were then repeated in a cooling sequence back down to room temperature. Lattice parameter and $\Sigma I_b/\Sigma I_a$ data from the heating and cooling cycles are given in Table 4.

TABLE 2. Variation of the aggregate intensity ratios ($\Sigma I_b/\Sigma I_a$) with T for pigeonite crystal BTS-308 n.17, before (1) and after (2–5) each ex-situ heat treatment at successively higher temperatures

In-situ T(°C)	1	2 (700 °C)	3 (750 °C)	4 (800 °C)	5 (850 °C)
28	0.251	0.293	0.271	0.304	0.306
50	0.247	0.289	0.268	0.301	0.301
75	0.242	0.285	0.261	0.294	0.292
100	0.237	0.274	0.254	0.287	0.289
125	0.231	0.268	0.249	0.279	0.272
150	0.225	0.260	0.242	0.271	0.272
175	0.219	0.258	0.233	0.262	0.270
200	0.214	0.249	0.231	0.258	0.260
225	0.207	0.241	0.218	0.251	0.252
250	0.201	0.236	0.217	0.243	0.247
275	0.194	0.228	0.207	0.234	0.239
300	0.186	0.222	0.202	0.228	0.217
325	0.181	0.214	0.193	0.220	0.215
350	0.174	0.204	0.187	0.212	0.195
375	0.167	0.197	0.178	0.205	0.193
400	0.160	0.189	0.172	0.196	0.186
425	0.152	0.184	0.164	0.188	0.185
450	0.146	0.174	0.155	0.179	0.175
475	0.137	0.164	0.148	0.170	0.166
500	0.128	0.157	0.138	0.159	0.157

DATA COLLECTION AND STRUCTURE REFINEMENT

In order to determine the degree of Fe/Mg order between M1 and M2 sites, a complete data collection was performed on natural crystal BTS-308 no. 17 prior to any heat treatments. This was repeated after each ex situ annealing experiment. The X-ray diffraction intensity data were collected with a Philips PW1100 automated 4-circle diffractometer equipped with graphite-monochromatized Mo$K\alpha$ X-radiation and working at 55 kV and 30 mA. Two equivalent monoclinic reflections (hkl and $h\bar{k}l$) were collected in the θ range 2–35°. Intensity profiles were integrated following the method of Lehmann and Larsen (1974), modified by Blessing et al. (1974). Intensities were corrected for Lorentz and polarization factors, and for absorption following North et al. (1968). Unit-cell dimensions were calculated using a locally improved version (Cannillo et al. 1983) of the Philips LAT routine by centering 50 reflections in the range $-35 < \theta < 35°$. Weighted full-matrix least-squared refinements were completed using SHELX-97 (Sheldrick 1997). Scattering factors were taken from the *International Tables for X-ray Crystallography* (Hahn 1995; Wilson 1995). Neutral vs. ionized scattering factors were refined in all the sites that are not involved in chemical substitutions (Hawthorne et al. 1995). Cation site assignments were achieved using a modified version of the routine MINUIT (Zema et al. 1997). Lattice parameters and information from the structure refinements are reported in Table 5. After annealing at 800 °C the crystal broke and its volume was reduced (see crystal dimensions in Table 5), giving an increase in the number of low-intensity reflections. This explains the significantly increased value of discrepancy factors, R(all), obtained in the last structure refinements. Positional and isotropic displacement parameters are reported in Table 6a. Anisotropic displacement parameters are reported in Table 6b[1], which has been deposited. Selected bond lengths and angles are reported in Table 7. Observed and calculated structure factors are reported in Table 8[1]. Values of site populations, the equilibrium distribution coefficient, K_D (from Eq. 19), and the order parameter, Q_{OD} (from Eqs. 14, 17 and 18) are reported in Table 9.

ANALYSIS AND DISCUSSION

Spontaneous strains

Lattice parameters for crystal BTS-308 no. 14 from Table 4 are shown as a function of temperature in Figure 1. Values for the baseline parameters, a_o, b_o, c_o, β_o, and V_o, were obtained by fitting straight lines to the data for a, b, c, sinβ and V at 875, 900, 950, 1000, and 1050 °C. These fits gave

$$a_o = 9.7000 + 0.0001267.T \text{ (Å)} \quad (26)$$
$$b_o = 8.9020 + 0.0001094.T \text{ (Å)} \quad (27)$$
$$c_o = 5.2756 + 0.00003658.T \text{ (Å)} \quad (28)$$
$$\sin\beta_o = 0.9462 - 0.000002515.T \quad (29)$$
$$V_o = 430.85 + 0.01304.T \text{ (Å}^3\text{)} \quad (30)$$

for T in Kelvins. Many significant figures are given here to avoid rounding errors and not to signify the precision of the fit

[1]For a copy of Table 6b and Table 8, document item AM-03-037, contact the Business Office of the Mineralogical Society of America (see inside front cover of recent issue) for price information. Deposit items may also be available on the American Mineralogist web site at http://www.minsocam.org.

TABLE 3. Lattice parameters for crystal BTS-308 n.17

T_{eq}*	T(°C)	a (Å)	b (Å)	c (Å)	β (°)	V(Å³)
630	28	9.714 (4)	8.949 (4)	5.249 (2)	108.52 (3)	432.7 (3)
	50	9.718 (3)	8.951 (2)	5.251 (2)	108.54 (2)	433.0 (2)
	75	9.721 (4)	8.953 (2)	5.252 (1)	108.56 (2)	433.4 (2)
	100	9.727 (6)	8.956 (5)	5.254 (1)	108.61 (3)	433.8 (4)
	125	9.727 (3)	8.958 (3)	5.255 (2)	108.60 (2)	434.0 (3)
	150	9.730 (4)	8.961 (3)	5.257 (2)	108.61 (3)	434.3 (3)
	175	9.733 (3)	8.963 (3)	5.258 (2)	108.63 (2)	434.7 (3)
	200	9.736 (4)	8.965 (4)	5.259 (1)	108.65 (2)	434.9 (3)
	225	9.739 (3)	8.968 (3)	5.261 (2)	108.67 (2)	435.3 (3)
	250	9.742 (4)	8.970 (3)	5.263 (2)	108.68 (4)	435.7 (3)
	275	9.745 (3)	8.973 (3)	5.264 (2)	108.70 (2)	436.0 (3)
	300	9.749 (5)	8.975 (5)	5.266 (2)	108.70 (3)	436.4 (4)
	325	9.751 (3)	8.978 (3)	5.267 (2)	108.73 (2)	436.7 (3)
	350	9.754 (4)	8.980 (2)	5.268 (2)	108.75 (3)	437.0 (3)
	375	9.757 (3)	8.983 (3)	5.270 (2)	108.77 (2)	437.3 (3)
	400	9.759 (6)	8.985 (4)	5.271 (1)	108.77 (3)	437.6 (3)
	425	9.763 (4)	8.988 (3)	5.273 (2)	108.80 (3)	438.0 (3)
	450	9.765 (5)	8.989 (4)	5.275 (1)	108.82 (2)	438.3 (3)
	475	9.769 (3)	8.992 (3)	5.276 (2)	108.84 (2)	438.6 (3)
	500	9.774 (4)	8.996 (4)	5.277 (1)	108.88 (2)	439.0 (3)
700	25	9.721 (8)	8.951 (6)	5.251 (2)	108.51 (4)	433.3 (5)
	50	9.723 (6)	8.953 (7)	5.251 (1)	108.51 (4)	433.5 (4)
	75	9.726 (7)	8.956 (6)	5.256 (2)	108.54 (4)	434.1 (5)
	100	9.727 (6)	8.959 (7)	5.256 (2)	108.56 (4)	434.2 (5)
	125	9.729 (6)	8.960 (6)	5.256 (1)	108.59 (3)	434.3 (4)
	150	9.734 (7)	8.964 (6)	5.257 (2)	108.60 (4)	434.7 (5)
	175	9.737 (6)	8.967 (5)	5.260 (2)	108.62 (4)	435.2 (4)
	200	9.738 (6)	8.966 (5)	5.260 (2)	108.61 (4)	435.2 (4)
	225	9.745 (6)	8.973 (6)	5.264 (1)	108.65 (3)	436.1 (4)
	250	9.744 (5)	8.974 (6)	5.265 (2)	108.66 (3)	436.2 (4)
	275	9.750 (6)	8.977 (6)	5.267 (2)	108.68 (3)	436.7 (4)
	300	9.753 (6)	8.977 (7)	5.266 (2)	108.71 (4)	436.7 (5)
	325	9.757 (6)	8.981 (7)	5.271 (1)	108.74 (3)	437.4 (4)
	350	9.759 (5)	8.983 (5)	5.271 (2)	108.75 (3)	437.6 (4)
	375	9.763 (6)	8.987 (6)	5.272 (1)	108.74 (3)	438.0 (4)
	400	9.766 (6)	8.988 (6)	5.274 (2)	108.78 (4)	438.3 (4)
	425	9.770 (6)	8.990 (7)	5.277 (2)	108.82 (3)	438.7 (5)
	450	9.775 (6)	8.993 (7)	5.280 (2)	108.84 (4)	439.3 (5)
	475	9.777 (7)	8.996 (5)	5.283 (1)	108.86 (3)	439.7 (4)
	500	9.780 (8)	8.999 (5)	5.283 (1)	108.86 (4)	440.0 (5)
750	25	9.715 (7)	8.948 (4)	5.249 (2)	108.49 (5)	432.7 (4)
	50	9.719 (5)	8.950 (4)	5.249 (2)	108.50 (4)	433.0 (4)
	75	9.723 (5)	8.952 (5)	5.251 (2)	108.55 (3)	433.3 (4)
	100	9.725 (6)	8.955 (4)	5.252 (2)	108.53 (4)	433.7 (4)
	125	9.726 (5)	8.957 (4)	5.253 (2)	108.56 (4)	433.8 (4)
	150	9.731 (5)	8.962 (4)	5.256 (2)	108.58 (4)	434.5 (4)
	175	9.734 (6)	8.963 (4)	5.257 (2)	108.59 (4)	434.7 (4)
	200	9.737 (5)	8.964 (4)	5.258 (2)	108.60 (4)	435.0 (4)
	225	9.737 (5)	8.969 (4)	5.260 (3)	108.64 (5)	435.3 (4)
	250	9.743 (5)	8.970 (5)	5.261 (3)	108.64 (4)	435.7 (4)
	275	9.745 (6)	8.974 (4)	5.264 (2)	108.68 (5)	436.1 (4)
	300	9.749 (5)	8.977 (4)	5.265 (2)	108.69 (3)	436.5 (3)
	325	9.751 (6)	8.979 (4)	5.266 (2)	108.70 (5)	436.7 (4)
	350	9.755 (6)	8.980 (5)	5.270 (2)	108.72 (4)	437.2 (4)
	375	9.759 (6)	8.985 (4)	5.271 (2)	108.73 (4)	437.7 (4)
	400	9.762 (5)	8.985 (4)	5.271 (2)	108.76 (4)	437.8 (4)
	425	9.767 (6)	8.989 (4)	5.276 (3)	108.80 (4)	438.5 (4)
	450	9.769 (5)	8.991 (3)	5.279 (2)	108.81 (4)	438.9 (3)
	475	9.776 (6)	8.995 (4)	5.281 (3)	108.86 (4)	439.5 (4)
	500	9.776 (5)	8.995 (4)	5.281 (2)	108.87 (3)	439.4 (4)
800	25	9.717 (3)	8.954 (3)	5.252 (2)	108.50 (2)	433.3 (3)
	50	9.720 (3)	8.956 (2)	5.254 (2)	108.52 (2)	433.7 (2)
	75	9.722 (4)	8.958 (2)	5.253 (1)	108.51 (2)	433.8 (2)
	100	9.724 (4)	8.962 (1)	5.254 (1)	108.52 (2)	434.2 (2)
	125	9.728 (3)	8.964 (3)	5.256 (2)	108.55 (2)	434.5 (3)
	150	9.729 (4)	8.967 (3)	5.258 (2)	108.57 (3)	434.8 (3)
	175	9.732 (3)	8.969 (3)	5.260 (2)	108.58 (2)	435.2 (3)
	200	9.738 (3)	8.973 (3)	5.260 (2)	108.59 (2)	435.6 (3)
	225	9.738 (3)	8.976 (3)	5.262 (2)	108.61 (2)	435.9 (3)
	250	9.743 (4)	8.975 (3)	5.264 (2)	108.64 (4)	436.2 (3)
	275	9.745 (3)	8.980 (3)	5.264 (2)	108.65 (2)	436.5 (3)
	300	9.750 (4)	8.982 (2)	5.269 (1)	108.68 (3)	437.1 (2)
	325	9.753 (3)	8.985 (3)	5.268 (2)	108.69 (2)	437.3 (3)
	350	9.756 (4)	8.988 (2)	5.271 (2)	108.71 (3)	437.8 (3)
	375	9.760 (3)	8.990 (3)	5.272 (2)	108.73 (2)	438.1 (3)
	400	9.763 (4)	8.992 (3)	5.273 (2)	108.74 (3)	438.4 (3)
	425	9.767 (4)	8.995 (3)	5.276 (2)	108.77 (3)	438.9 (3)
	450	9.768 (3)	8.997 (3)	5.277 (2)	108.79 (3)	439.0 (3)
	475	9.775 (3)	9.000 (3)	5.279 (2)	108.81 (2)	439.6 (3)
	500	9.777 (4)	9.001 (3)	5.283 (1)	108.85 (3)	440.0 (3)
850	25	9.719 (3)	8.950 (3)	5.251 (2)	108.56 (2)	433.0 (3)
	50	9.719 (3)	8.950 (2)	5.251 (2)	108.51 (2)	433.1 (2)
	75	9.719 (4)	8.954 (2)	5.253 (1)	108.54 (2)	433.4 (2)
	100	9.723 (4)	8.954 (1)	5.254 (1)	108.57 (2)	433.6 (2)
	125	9.726 (3)	8.958 (3)	5.254 (2)	108.58 (2)	433.9 (3)
	150	9.730 (4)	8.960 (3)	5.257 (2)	108.63 (3)	434.3 (3)
	175	9.734 (3)	8.965 (3)	5.258 (2)	108.65 (2)	434.7 (3)
	200	9.736 (3)	8.966 (3)	5.259 (2)	108.63 (2)	435.0 (3)
	225	9.741 (3)	8.970 (3)	5.261 (2)	108.70 (2)	435.4 (3)
	250	9.739 (4)	8.970 (3)	5.261 (2)	108.66 (4)	435.4 (3)
	275	9.744 (3)	8.974 (3)	5.264 (2)	108.72 (2)	436.0 (3)
	300	9.748 (4)	8.976 (2)	5.265 (1)	108.74 (3)	436.3 (2)
	325	9.751 (3)	8.980 (3)	5.266 (2)	108.73 (2)	436.7 (3)
	350	9.759 (4)	8.983 (2)	5.269 (2)	108.79 (3)	437.3 (3)
	375	9.759 (3)	8.984 (3)	5.273 (2)	108.80 (2)	437.7 (3)
	400	9.763 (4)	8.989 (3)	5.272 (2)	108.80 (3)	438.0 (3)
	425	9.765 (4)	8.990 (3)	5.278 (2)	108.81 (3)	438.6 (3)
	450	9.770 (3)	8.994 (3)	5.279 (2)	108.86 (3)	439.0 (3)
	475	9.777 (3)	8.998 (3)	5.281 (2)	108.89 (2)	439.6 (3)
	500	9.776 (4)	8.996 (3)	5.282 (1)	108.91 (3)	439.5 (3)

* T_{eq} = temperature of equilibrium Q_{OD}.

TABLE 4. Lattice parameters and intensity data for pigeonite crystal BTS-308 n.14

T(°C)	a (Å)	b (Å)	c (Å)	β (°)	V(Å³)	I_b/I_a
28	9.714 (4)	8.949 (4)	5.249 (2)	108.52 (3)	432.7 (3)	0.251
100	9.727 (6)	8.956 (5)	5.254 (1)	108.61 (3)	433.8 (4)	0.237
200	9.736 (4)	8.965 (4)	5.259 (1)	108.65 (2)	434.9 (3)	0.214
300	9.749 (5)	8.975 (5)	5.266 (2)	108.70 (3)	436.4 (4)	0.186
400	9.759 (6)	8.985 (4)	5.271 (1)	108.77 (3)	437.6 (3)	0.160
450	9.765 (5)	8.989 (4)	5.275 (1)	108.82 (2)	438.3 (3)	0.146
500	9.774 (4)	8.996 (4)	5.277 (1)	108.88 (2)	439.0 (3)	0.128
550	9.780 (4)	8.999 (4)	5.283 (2)	108.90 (3)	439.9 (3)	0.114
600	9.789 (5)	9.006 (5)	5.288 (1)	108.97 (3)	440.9 (4)	0.097
650	9.796 (3)	9.010 (4)	5.292 (2)	109.02 (2)	441.6 (3)	0.080
675	9.803 (4)	9.009 (4)	5.295 (2)	109.08 (2)	442.0 (3)	0.072
700	9.806 (4)	9.014 (4)	5.298 (2)	109.10 (3)	442.5 (3)	0.064
725	9.810 (6)	9.013 (5)	5.301 (2)	109.15 (3)	442.8 (4)	0.052
750	9.817 (5)	9.019 (5)	5.302 (2)	109.19 (3)	443.4 (4)	0.043
775	9.820 (4)	9.018 (4)	5.305 (1)	109.23 (2)	443.6 (3)	0.036
800	9.828 (5)	9.020 (5)	5.309 (2)	109.29 (3)	444.2 (4)	0.028
825	9.831 (4)	9.023 (4)	5.312 (1)	109.30 (2)	444.7 (3)	0.021
850	9.836 (4)	9.026 (3)	5.313 (1)	109.33 (3)	445.1 (3)	0.016
875	9.843 (5)	9.031 (5)	5.317 (2)	109.37 (3)	445.9 (4)	0.010
900	9.847 (5)	9.031 (4)	5.317 (2)	109.37 (3)	446.1 (4)	0.008
950	9.855 (5)	9.039 (6)	5.322 (2)	109.42 (3)	447.1 (4)	0.005
1000	9.861 (2)	9.041 (5)	5.319 (1)	109.43 (3)	447.2 (3)	0.005
1050	9.865 (6)	9.047 (4)	5.324 (2)	109.46 (3)	448.0 (4)	0.006
1000	9.868 (5)	9.040 (4)	5.324 (1)	109.49 (2)	447.7 (3)	0.005
950	9.857 (4)	9.034 (3)	5.321 (1)	109.45 (2)	446.8 (3)	0.005
900	9.849 (5)	9.028 (5)	5.319 (1)	109.42 (3)	446.0 (4)	0.006
875	9.846 (5)	9.025 (4)	5.318 (1)	109.41 (3)	445.7 (3)	0.008
850	9.842 (4)	9.024 (4)	5.315 (1)	109.40 (2)	445.3 (3)	0.010
825	9.838 (4)	9.020 (4)	5.316 (1)	109.39 (2)	445.0 (3)	0.010
800	9.834 (6)	9.018 (5)	5.313 (1)	109.37 (3)	444.5 (4)	0.015
775	9.830 (6)	9.014 (6)	5.313 (2)	109.35 (4)	444.2 (4)	0.019
750	9.824 (4)	9.013 (4)	5.310 (2)	109.28 (2)	443.8 (3)	0.026
725	9.819 (5)	9.005 (5)	5.305 (1)	109.26 (4)	442.8 (4)	0.032
700	9.810 (4)	9.010 (5)	5.302 (2)	109.19 (3)	442.6 (4)	0.043
675	9.810 (6)	9.008 (4)	5.301 (1)	109.18 (3)	442.4 (4)	0.051
650	9.803 (6)	9.003 (5)	5.298 (2)	109.16 (3)	441.7 (4)	0.062
600	9.792 (5)	8.998 (5)	5.291 (1)	109.05 (2)	440.7 (3)	0.087
550	9.783 (5)	8.995 (5)	5.286 (1)	108.99 (3)	439.8 (4)	0.108
500	9.776 (5)	8.990 (5)	5.281 (1)	108.92 (3)	439.1 (4)	0.127
450	9.771 (5)	8.986 (5)	5.277 (2)	108.90 (3)	438.4 (4)	0.144
400	9.760 (5)	8.982 (4)	5.273 (1)	108.82 (2)	437.5 (3)	0.158
300	9.749 (7)	8.971 (5)	5.266 (1)	108.77 (3)	436.1 (4)	0.192
200	9.733 (9)	8.961 (7)	5.260 (2)	108.70 (5)	434.6 (6)	0.218
100	9.722 (7)	8.948 (5)	5.252 (1)	108.62 (3)	433.0 (4)	0.246
25	9.716 (6)	8.949 (5)	5.250 (1)	108.56 (3)	432.7 (4)	0.262

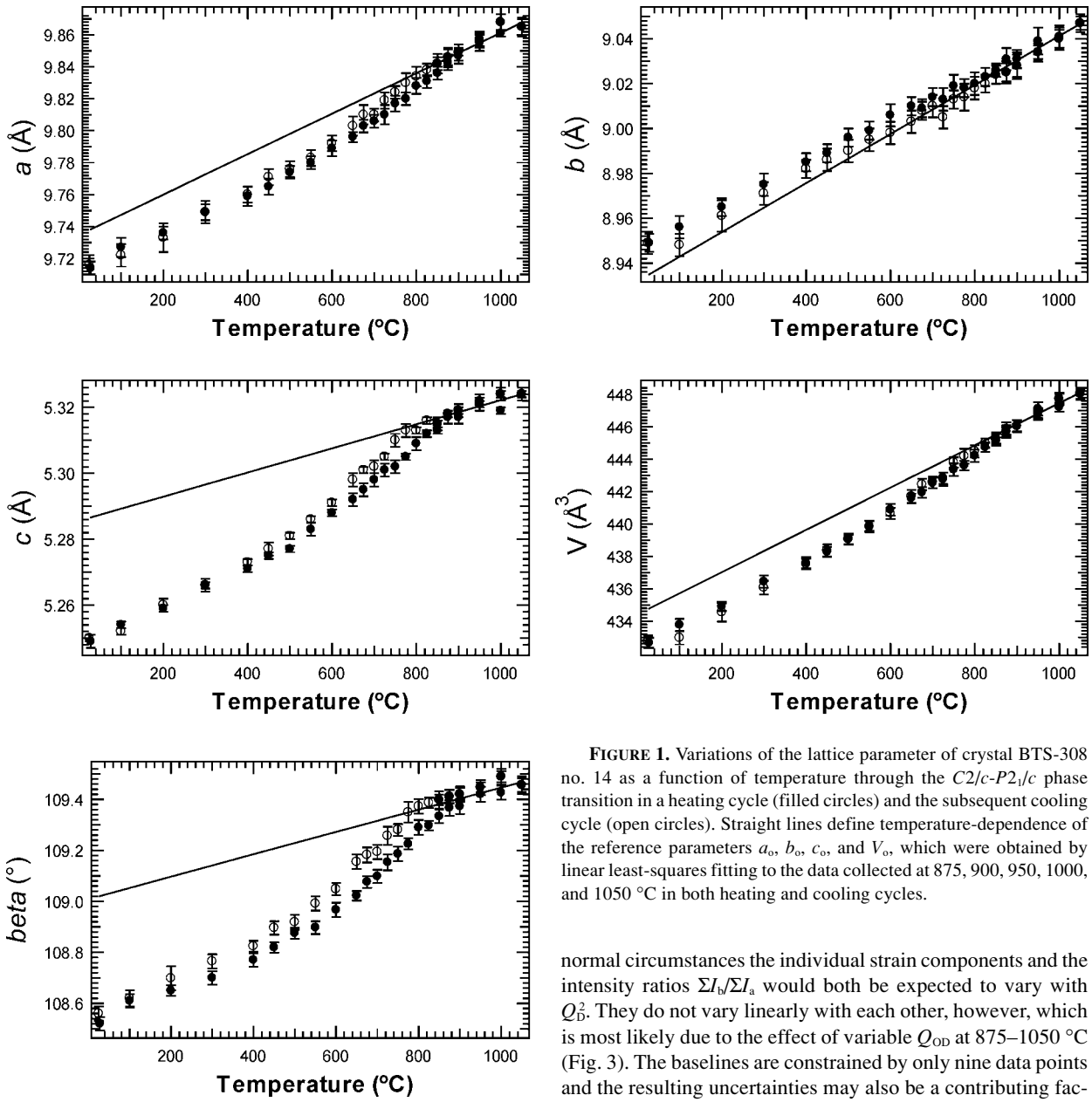

FIGURE 1. Variations of the lattice parameter of crystal BTS-308 no. 14 as a function of temperature through the $C2/c$-$P2_1/c$ phase transition in a heating cycle (filled circles) and the subsequent cooling cycle (open circles). Straight lines define temperature-dependence of the reference parameters a_o, b_o, c_o, and V_o, which were obtained by linear least-squares fitting to the data collected at 875, 900, 950, 1000, and 1050 °C in both heating and cooling cycles.

parameters. Individual strain parameters were then calculated according to Equations 20–25, and the results are plotted in Figure 2. All the strains show a continuous, but non-linear, decrease from their room temperature values to ~0 above 1050–1100 K. Differences between the heating and cooling cycles show that irreversible structural changes occurred in the pigeonite crystal at high temperatures.

An important limitation in this strain analysis arises from the fact that, while the reference parameters, a_o, b_o, etc., refer to structural states with $Q_D = 0$, they do not have $Q_{OD} = 0$. It is also probable that changes in the lattice parameters between the heating and cooling cycles are due to changes in Q_{OD} on the time scale of the measurements at high temperatures. Thus the baseline parameters do not even refer to constant Q_{OD}. Under normal circumstances the individual strain components and the intensity ratios $\Sigma I_b/\Sigma I_a$ would both be expected to vary with Q_D^2. They do not vary linearly with each other, however, which is most likely due to the effect of variable Q_{OD} at 875–1050 °C (Fig. 3). The baselines are constrained by only nine data points and the resulting uncertainties may also be a contributing factor. In spite of these limitations, the strain data show semi-quantitative trends for the effects of the $C2/c$-$P2_1/c$ transition. Diagonalization of the strain matrix gives principal strains, ε_1, ε_2, ε_3, parallel to the crystallographic **y**-axis and approximately midway between the crystallographic **x**- and **c***-axes (Fig. 4). The largest component, ε_3, is a contraction while ε_1 and ε_2 are expansions, and there is a significant component of shear in the (010) plane ($\varepsilon_1 - \varepsilon_3 \approx 1\%$ at room temperature). There is a small negative volume strain overall, which amounts to ~5% at room temperature. The orientations of the principal strains do not vary significantly as a function of temperature.

Lattice parameters for each of the in situ sequences of measurements from crystal BTS-308 no. 17 represent sets of data for different fixed values of Q_{OD}. The individual lattice parameters are plotted against $\Sigma I_b/\Sigma I_a$ in Figure 5, from which it is

TABLE 5. Lattice parameters and results of structure refinements of pigeonite BTS-308 n.17 before (1) and after (2-5) ex-situ heat treatment as successively higher temperatures. The final set of data (6) was obtained from the crystal after the final in-situ run to 500 °C

Sample	1	2	3	4	5	6
ex-situ *T*(°C)		700	750	800	850	850
CNR-IGG code	hem	hks	hkc	hlo	hqu	hxv
a (Å)	9.716(5)	9.708(3)	9.707(2)	9.707(2)	9.711(5)	9.718(1)
b (Å)	8.946(5)	8.941(3)	8.941(2)	8.943(2)	8.944(3)	8.951(1)
c (Å)	5.252(4)	5.244(2)	5.247(1)	5.246(1)	5.249(3)	5.250(1)
β (°)	108.49(5)	108.52(3)	108.48(2)	108.47(2)	108.49(4)	108.50(1)
Volume (Å^3)	432.9(8)	431.6(2)	431.9(2)	431.9(2)	432.4(3)	433.1(1)
Crystal size mm^3	0.330 x	0.330 x	0.330 x	0.330 x	0.165 x	0.165 x
	0.264 x	0.264 x	0.264 x	0.264 x	0.132 x	0.132 x
	0.198	0.198	0.198	0.198	0.050	0.050
θrange (°)	2.21 to 35	2.21 to 35	2.21 to 35	2.21 to 35	2.21 to 35	2.21 to 35
Index ranges	−16<*h*<15,	−16<*h*<15,	−16<*h*<15,	−16<*h*<15,	−16<*h*<15,	−16<*h*<15,
	−15<*k*<15,	−15<*k*<15,	−15<*k*<15,	−15<*k*<15,	−15<*k*<15,	−15<*k*<15,
	0=*l*<9	0=*l*<9	0=*l*<9	0=*l*<9	0=*l*<9	0=*l*<9
*/**	4045	4038	4053	4046	4161	4162
Iu†	1912	1911	1916	1913	1913	1914
R(int)	0.0310	0.0150	0.0180	0.0158	0.0340	0.0791
Data / parameter	1912 /105	1911 /105	1916 /105	1913 /105	1913 /105	1914 /105
S‡	1.031	1.023	1.025	1.048	0.794	0.753
*R*1 (4σ)	0.0320	0.0271	0.0307	0.0251	0.0277	0.0432
*R*1 (all)	0.0430	0.0340	0.0372	0.0317	0.0703	0.1348
w*R*2 (all)	0.0890	0.0711	0.0835	0.0583	0.0505	0.0624
P & *H* (e^{-3}) ‖	1.538 &	1.451 &	1.374 &	1.254 &	0.804 &	0.821 &
	−1.131	−1.076	−1.347	−1.020	−0.579	−0.615

* */* = number of reflections collected.
† *Iu* = number of unique reflections.
‡ *S* = goodness-of-fit on F^2.
‖ *P* & *H* = largest diffraction peak and hole.

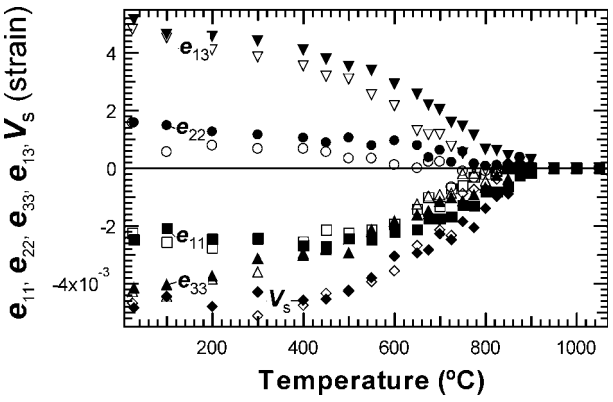

FIGURE 2. Variations of the spontaneous strains for crystal BTS-308 no. 14 as a function of temperature through the $C2/c$-$P2_1/c$ phase transition in a heating cycle (filled symbols) and the subsequent cooling cycle (open symbols). The propagated experimental uncertainty for these data is given by ± 1σ ≈ ± 0.001.

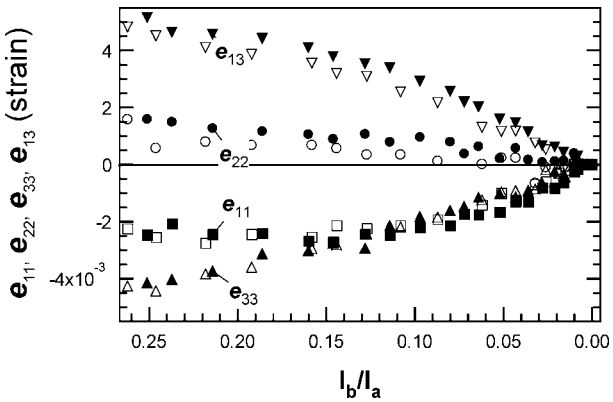

FIGURE 3. Variations of the spontaneous strains for crystal BTS-308 no. 14 as a function of the intensity ratio, $\Sigma I_b/\Sigma I_a$, for the heating cycle (filled symbols) and the subsequent cooling cycle (open symbols). Both of these experimental parameters are expected to vary with Q_D^2, unless there are contributions to the strain due to variations in Q_{OD}. The non-linear relationships are consistent with changes in Q_{OD} occurring at high temperatures during data collection.

possible to extract variations of a, b, c, β, and V as a function of Q_{OD} at constant Q_D. In each case, the individual lattice parameters show linear variations and the separate data sets define more or less parallel trends. For the a parameter, straight lines were first fit to each data set. An average slope was determined and the straight lines refit to the data with the slope held constant at this average value. Values of a were then taken from the linear fits at $\Sigma I_b/\Sigma I_a = 0.25$ and plotted against the corresponding Q_{OD} (Fig. 6). By fitting lines of constant slope through the different data sets, it is assumed that the strength of strain coupling with Q_{OD} is independent of the value of Q_D. This procedure was repeated for each of b, c, sinβ, and V and the resulting variations with Q_{OD} are included in Figure 6. A linear relationship between the lattice parameters and Q_{OD} is expected if the strain coupling is of the form $\lambda e_{ik} Q_{OD}$. The data in Figure 6 show much greater scatter than those in Figure 1 because of the way the lattice parameters were collected. Once centered, a single crystal gives internally consistent changes in lattice parameters when the temperature is changed. The greater scatter arising from remounting and recentering the crystal between

TABLE 6A. Atomic coordinates and equivalent isotropic displacement parameters (Å²) for crystal BTS-308 n.17 before (1) and after (2–5) ex-situ heat treatments at successively higher temperatures; the final data set (6) was obtained from data collected after the final in-situ run to 500 °C

Sample		1	2	3	4	5	6
ex-situ T(°C)			700	750	800	850	850
O1A	x	–0.1326(1)	–0.1327(1)	-0.1326(1)	–0.1326(1)	–0.1324(2)	–0.1326(3)
	y	0.3381(2)	0.3384(1)	0.3385(1)	0.3386(1)	0.3385(2)	0.3384(4)
	z	0.1688(3)	0.1699(2)	0.1699(2)	0.1705(2)	0.1710(3)	0.1704(5)
	U_{eq}	0.008(1)	0.008(1)	0.008(1)	0.008(1)	0.008(1)	0.007(1)
O1b	X	0.3736(1)	0.3737(1)	0.3738(1)	0.3738(1)	0.3738(2)	0.3734(3)
	Y	0.8364(2)	0.8368(1)	0.8369(1)	0.8369(1)	0.8371(2)	0.8374(3)
	Z	0.1344(3)	0.1339(2)	0.1343(2)	0.1341(2)	0.1334(3)	0.1339(5)
	U_{eq}	0.008(1)	0.008(1)	0.009(1)	0.008(1)	0.008(1)	0.007(1)
O2A	x	0.1218(2)	0.1217(1)	0.1217(1)	0.1217(1)	0.1216(2)	0.1220(3)
	y	0.4994(2)	0.4995(1)	0.4996(1)	0.4995(1)	0.4995(2)	0.4997(3)
	z	0.3324(3)	0.3318(2)	0.3316(2)	0.3315(2)	0.3307(3)	0.3315(6)
	U_{eq}	0.010(1)	0.010(1)	0.011(1)	0.010(1)	0.010(1)	0.009(1)
O2B	x	0.6288(2)	0.6293(1)	0.6293(1)	0.6294(1)	0.6287(2)	0.6281(3)
	y	0.9879(2)	0.9875(1)	0.9874(1)	0.9874(1)	0.9875(2)	0.9868(3)
	z	0.3726(3)	0.3740(3)	0.3737(3)	0.3741(2)	0.3729(3)	0.3717(6)
	U_{eq}	0.014(1)	0.014(1)	0.014(1)	0.013(1)	0.014(1)	0.014(1)
O3A	x	0.1043(2)	0.1043(1)	0.1045(1)	0.1041(1)	0.1041(2)	0.1041(3)
	y	0.2391(2)	0.2375(2)	0.2372(2)	0.2370(1)	0.2369(2)	0.2370(3)
	z	0.0765(3)	0.0795(3)	0.0799(3)	0.0802(2)	0.0802(3)	0.0798(5)
	U_{eq}	0.018(1)	0.016(1)	0.017(1)	0.016(1)	0.014(1)	0.012(1)
O3B	x	0.6050(2)	0.6051(1)	0.6050(1)	0.6049(1)	0.6047(2)	0.6043(3)
	y	0.7097(2)	0.7086(1)	0.7086(2)	0.7084(1)	0.7089(2)	0.7098(3)
	z	0.4808(3)	0.4795(2)	0.4791(2)	0.4791(2)	0.4800(3)	0.4800(5)
	U_{eq}	0.013(1)	0.013(1)	0.014(1)	0.013(1)	0.012(1)	0.011(1)
SiA	x	0.0426(1)	0.0426(1)	0.0427(1)	0.0426(1)	0.0426(1)	0.0424(1)
	y	0.3405(1)	0.3404(1)	0.3404(1)	0.3404(1)	0.3404(1)	0.3407(2)
	z	0.2761(1)	0.2775(1)	0.2776(1)	0.2780(1)	0.2783(1)	0.2780(2)
	U_{eq}	0.006(1)	0.006(1)	0.007(1)	0.006(1)	0.006(1)	0.006(1)
SiB	x	0.5494(1)	0.5496(1)	0.5496(1)	0.5497(1)	0.5497(1)	0.5498(1)
	y	0.8374(1)	0.8374(1)	0.8374(1)	0.8373(1)	0.8372(1)	0.8370(2)
	z	0.2386(1)	0.2380(1)	0.2382(1)	0.2380(1)	0.2379(1)	0.2377(2)
	U_{eq}	0.006(1)	0.006(1)	0.007(1)	0.006(1)	0.006(1)	0.005(1)
M1	x	0.2504(1)	0.2504(1)	0.2504(1)	0.2505(1)	0.2504(1)	0.2505(1)
	y	0.6547(1)	0.6546(1)	0.6546(1)	0.6546(1)	0.6545(1)	0.6546(1)
	z	0.2319(1)	0.2311(1)	0.2310(1)	0.2307(1)	0.2304(1)	0.2303(2)
	U_{eq}	0.006(1)	0.006(1)	0.007(1)	0.006(1)	0.007(1)	0.006(1)
M2	X	0.2552(1)	0.2553(1)	0.2554(1)	0.2554(1)	0.2554(1)	0.2554(1)
	Y	0.0190(1)	0.0188(1)	0.0188(1)	0.0187(1)	0.0191(1)	0.0194(1)
	Z	0.2294(1)	0.2286(1)	0.2286(1)	0.2283(1)	0.2282(1)	0.2281(2)
	U_{eq}	0.011(1)	0.011(1)	0.011(1)	0.011(1)	0.011(1)	0.011(1)

Note: U_{eq} is defined as one third of the trace of the orthogonalized U_{ij} tensor.

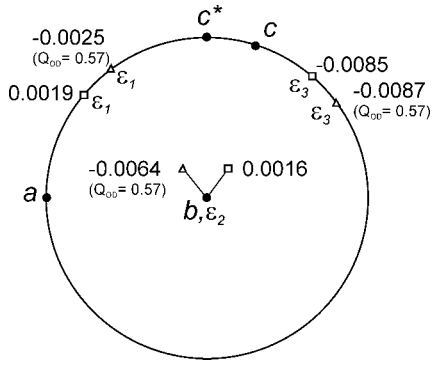

FIGURE 4. Stereogram showing the magnitudes and orientations of the principal strains due to coupling with Q_{OD} and Q_D. The data were calculated from the spontaneous strain components at room temperature for the $C2/c$-$P2_1/c$ transition and for Q_{OD} = 0.57 in the case strains due to Fe/Mg ordering. Reference axes are those specified by Carpenter et al. (1998) and used to derive Equations 20–24.

ex situ treatments is a reflection of the absolute uncertainty in the measurements. Given the scatter in the data and the limited range of Q_{OD} for which they are available, the analysis of strain coupling with the Fe/Mg ordering remains highly tentative. Semi-quantitative trends can perhaps be resolved. Straight line fits to the data in Figure 6 give values of a_o, b_o, etc., by extrapolation to Q_{OD} = 0, and these were used to calculate values for the strain components according to Equations 20–25. Diagonalization of the strain matrix, using values of the strain components for Q_{OD} = 0.57, gives the three principal strains shown in Figure 4. The total strain is dominated by a reduction in volume, with the largest contraction occurring in the plane containing ε_2 and ε_3.

At room temperature the total scalar strain, as defined by

$$\varepsilon_{ss} = \sqrt{\sum_{i,k} e_{ik}^2},$$

is ~0.011 for the phase transition and ~0.012 due to ordering from Q_{OD} = 0 to Q_{OD} = 0.57. Uncertainties on these values are

TABLE 7. Selected interatomic distances (Å) and angles (°) for crystal BTS-308 n.17 at room temperature before (1) and after (2–5) ex-situ heat treatments at successively higher temperatures; the final data set (6) was obtained from data collected after the final in-situ run to 500 °C

Sample	1	2	3	4	5	6
ex-situ T(°C)		700	750	800	850	850
SiA-O1A	1.615 (2)	1.614 (1)	1.614 (1)	1.614 (1)	1.612 (2)	1.613 (3)
SiA-O2A	1.599 (2)	1.598 (1)	1.599 (1)	1.598 (1)	1.598 (2)	1.601 (3)
SiA-O3A	1.636 (2)	1.637 (1)	1.637 (1)	1.637 (1)	1.641 (2)	1.643 (3)
SiA-O3A	1.660 (2)	1.658 (1)	1.660 (1)	1.658 (1)	1.657 (2)	1.659 (3)
<SiA-O>	1.628	1.627	1.628	1.627	1.627	1.629
TILT	3.83 (5)	3.75 (3)	3.71 (2)	3.78 (2)	3.75 (4)	3.84 (1)
SiB-O1B	1.620 (2)	1.619 (1)	1.618 (1)	1.619 (1)	1.620 (2)	1.626 (3)
SiB-O2B	1.600 (2)	1.600 (1)	1.598 (1)	1.600 (1)	1.597 (2)	1.592 (3)
SiB-O3B	1.663 (2)	1.662 (1)	1.664 (1)	1.662 (1)	1.658 (2)	1.656 (3)
SiB-O3B	1.668 (2)	1.669 (1)	1.668 (1)	1.669 (1)	1.670 (2)	1.664 (3)
<SiB-O>	1.638	1.638	1.637	1.638	1.636	1.634
TILT	5.62 (5)	5.71 (3)	5.75 (2)	5.77 (2)	5.66 (4)	5.64 (3)
M1-O1A	2.053 (2)	2.051 (1)	2.052 (1)	2.054 (1)	2.056 (2)	2.053 (3)
M1-O1A	2.157 (2)	2.157 (1)	2.159 (1)	2.159 (1)	2.160 (2)	2.161 (3)
M1-O1B	2.174 (2)	2.175 (1)	2.176 (1)	2.175 (1)	2.178 (2)	2.178 (3)
M1-O1B	2.074 (2)	2.073 (1)	2.077 (1)	2.076 (1)	2.076 (2)	2.077 (3)
M1-O2A	2.047 (2)	2.046 (1)	2.044 (1)	2.046 (1)	2.045 (2)	2.046 (3)
M1-O2B	2.076 (2)	2.075 (1)	2.075 (1)	2.075 (1)	2.076 (2)	2.082 (3)
<M1-O>	2.097	2.096	2.097	2.097	2.098	2.100
M2-O1A	2.174 (2)	2.169 (1)	2.168 (1)	2.168 (1)	2.172 (2)	2.177 (3)
M2-O1B	2.146 (2)	2.139 (1)	2.139 (1)	2.137 (1)	2.141 (2)	2.138 (3)
M2-O2A	2.083 (2)	2.079 (1)	2.083 (1)	2.082 (1)	2.086 (2)	2.082 (3)
M2-O2B	2.037 (2)	2.029 (2)	2.032 (2)	2.031 (2)	2.040 (2)	2.047 (3)
M2-O3A	3.443 (2)	3.464 (2)	3.466 (2)	3.472 (2)	3.472 (2)	3.472 (3)
M2-O3A	2.435 (2)	2.420 (2)	2.418 (2)	2.418 (2)	2.415 (2)	2.416 (3)
M2-O3B	2.957 (2)	2.967 (2)	2.969 (2)	2.971 (2)	2.965 (2)	2.960 (3)
M2-O3B	2.632 (2)	2.616 (1)	2.616 (1)	2.615 (1)	2.620 (2)	2.627 (3)
<M2-O> x6	2.251	2.242	2.243	2.242	2.246	2.248
<M2-O> x7	2.744	2.737	2.737	2.737	2.740	2.741
O3A-O3A-O3A	188.5 (2)	189.7 (1)	189.9 (1)	190.2 (1)	190.2 (1)	190.2 (2)
O3B-O3B-O3B	149.3 (1)	148.5 (1)	148.5 (1)	148.4 (1)	148.7 (1)	149.3 (2)

TABLE 9. Site occupancies calculated with MINUIT procedure for BTS-308 n.17 for each equilibration temperature

Sample	1	2	2	4	5	6
ex-situ T(°C)	636 *	700	750	800	850	850 †
s.s. M1(eps) ‡	15.07(6)	15.51(5)	15.64(5)	15.78(4)	15.93(4)	15.96(6)
s.s. M2 (eps)	22.33(7)	21.84(6)	21.76(6)	21.56(5)	21.19(5)	21.37(8)
Total eps	37.40	37.35	37.40	37.34	37.12	37.33
MgM1	0.7660	0.7340	0.7255	0.7161	0.7027	0.7016
FeM1	0.2105	0.2417	0.2501	0.2590	0.2712	0.2728
MnM1	0.0066	0.0076	0.0079	0.0081	0.0085	0.0086
TiM1	0.0097	0.0097	0.0097	0.0097	0.0097	0.0097
AlM1	0.0072	0.0072	0.0072	0.0072	0.0072	0.0072
CaM2	0.18	0.18	0.18	0.18	0.18	0.18
MgM2	0.1762	0.2105	0.2184	0.2317	0.2540	0.2420
FeM2	0.6231	0.5898	0.5822	0.5689	0.5464	0.5593
MnM2	0.0204	0.0194	0.0192	0.0189	0.0185	0.0185
X^{M1}_{Fe}	0.2208	0.2535	0.2623	0.2717	0.2847	0.2863
X^{M2}_{Fe}	0.7850	0.7432	0.7336	0.7173	0.6898	0.7048
X^{M1}_{Mg}	0.7792	0.7465	0.7377	0.7283	0.7153	0.7137
X^{M2}_{Mg}	0.2150	0.2568	0.2664	0.2827	0.3102	0.2952
K_D	0.0776	0.1174	0.1291	0.1470	0.1790	0.1680
Q_{OD}	0.568	0.488	0.469	0.441	0.395	0.415

* Untreated sample: T calculated with Pasqual et al. (2000) equation.
† After heating in-situ up to 500 °C.
‡ eps = electrons per site.

estimated to be ~±0.001 for the former, but much greater for the latter. They compare with an equivalent scalar strain of ~0.026 at room temperature for the phase transition in an Fe-free crystal (Tribaudino et al. 2002).

Order parameter coupling model

Of all the relationships derived from the initial Landau expansion, the two which are most readily tested using the experimental data are Equations 11 and 12. Variations of $\Sigma I_b/\Sigma I_a$ measured in situ as a function of temperature are shown in Figure 7. The intensities of $h + k = 2n + 1$ reflections are expected to scale with Q_D^2 for the $C2/c$-$P2_1/c$ transition, so the data give the temperature dependence of Q_D^2 at different fixed values of Q_{OD}. The intensity variations are non-linear, consistent with the solution to a 246 Landau potential. Curves through the data are fits using Equation 11, and values of the fit coefficients, T_{cD}^{**}, b_D^*/a_D, and c_D/a_D, are listed in Table 10. Data for pigeonite crystal number BTS-308 no. 14 are included in Figure 7 to

TABLE 10. Transition temperatures and Landau coefficients calculated from a polynomial fitting of $\Sigma I_b/\Sigma I_a$ vs. T (curves in Fig. 1)

Sample	Annealing T (°C)	Q_{OD}	T_{CD} (K)	b_D/a_D (K)	c_D/a_D (K)
BTS-308 n.17_1	636*	0.568	1031	1086	7208
BTS-308 n.17_2	700	0.488	1085	1224	4966
BTS-308 n.17_3	750	0.469	1093	1674	4547
BTS-308 n.17_4	800	0.441	1131	1683	3384
BTS-302 n.17_ 5	850	0.395	1160	2327	1331

* Equilibration temperature for natural sample calculated using the calibration of Pasqual et al. (2000).

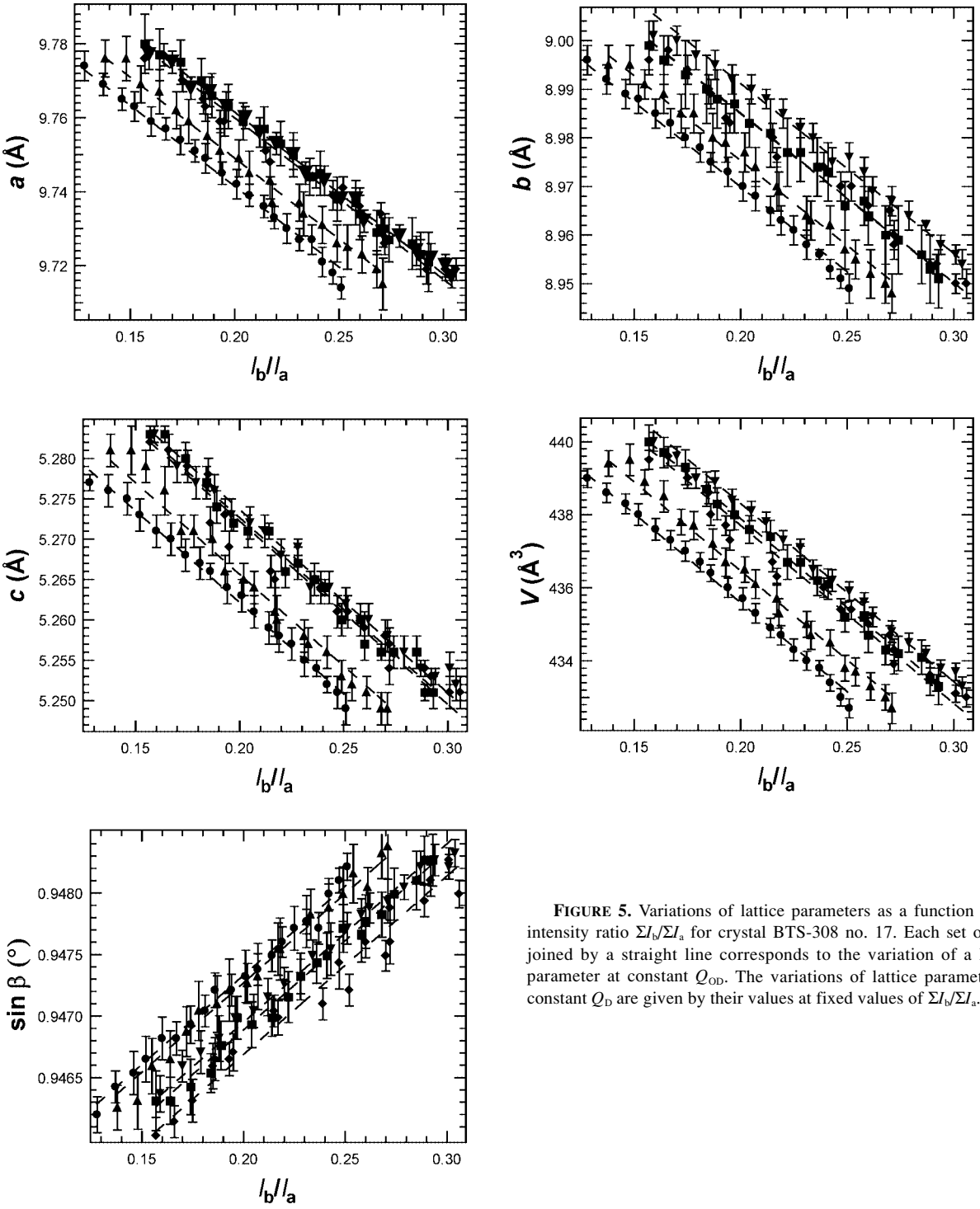

FIGURE 5. Variations of lattice parameters as a function of the intensity ratio $\Sigma I_b/\Sigma I_a$ for crystal BTS-308 no. 17. Each set of data joined by a straight line corresponds to the variation of a lattice parameter at constant Q_{OD}. The variations of lattice parameters at constant Q_D are given by their values at fixed values of $\Sigma I_b/\Sigma I_a$.

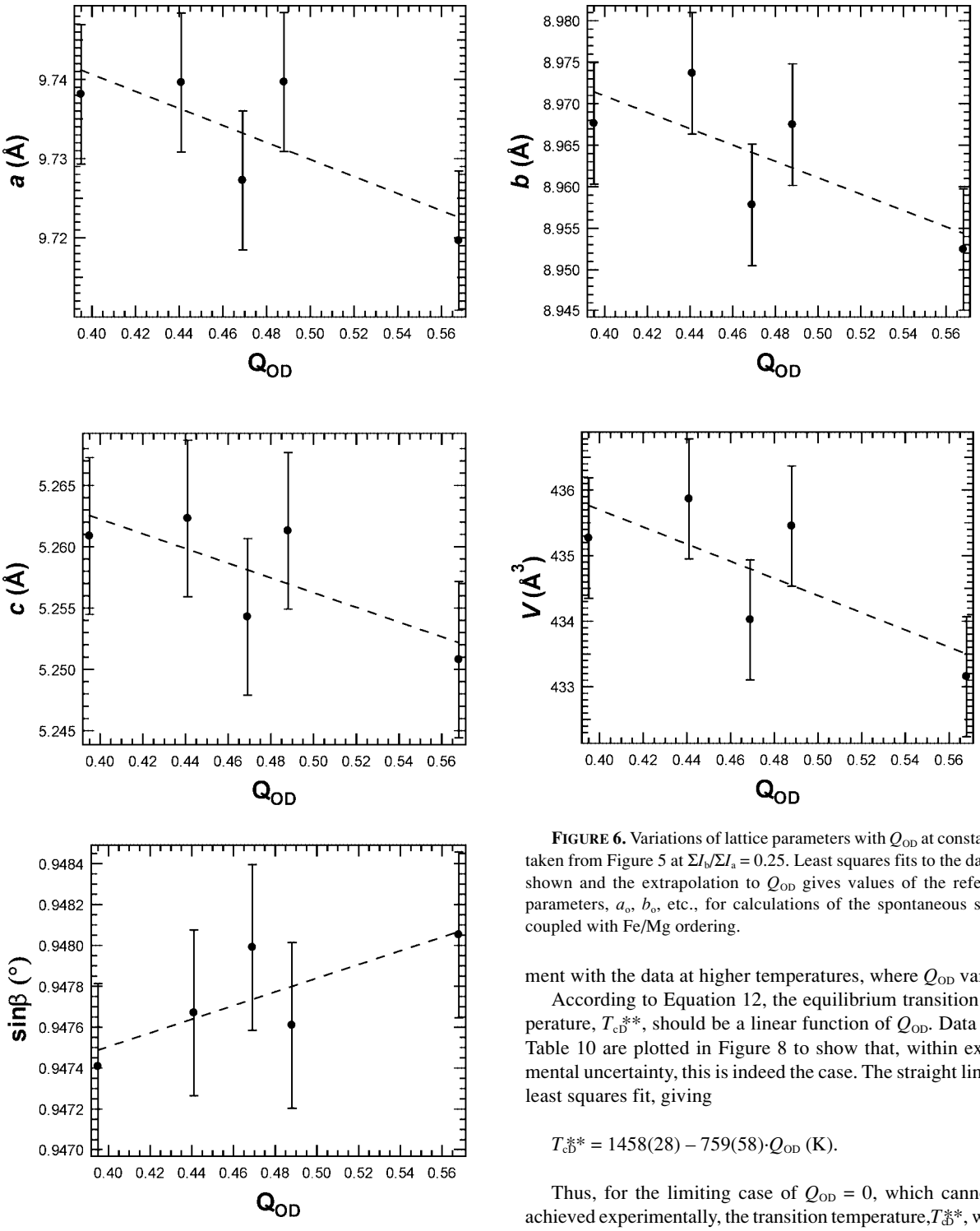

FIGURE 6. Variations of lattice parameters with Q_{OD} at constant Q_D taken from Figure 5 at $\Sigma I_b/\Sigma I_a = 0.25$. Least squares fits to the data are shown and the extrapolation to Q_{OD} gives values of the reference parameters, a_o, b_o, etc., for calculations of the spontaneous strains coupled with Fe/Mg ordering.

show that $\Sigma I_b/\Sigma I_a$ approaches zero continuously at higher temperatures. The evolution above ~773–873 K in this crystal is again complicated by the fact that Q_{OD} variations also occurred on the timescale of the intensity measurements. Fits using the 246 potential are reasonable for the temperature range up to ~900 K, where Q_{OD} is fixed, but show relatively poor agreement with the data at higher temperatures, where Q_{OD} varies.

According to Equation 12, the equilibrium transition temperature, T_{cD}^{**}, should be a linear function of Q_{OD}. Data from Table 10 are plotted in Figure 8 to show that, within experimental uncertainty, this is indeed the case. The straight line is a least squares fit, giving

$$T_{cD}^{**} = 1458(28) - 759(58)\cdot Q_{OD}\ (\mathrm{K}). \quad (31)$$

Thus, for the limiting case of $Q_{OD} = 0$, which cannot be achieved experimentally, the transition temperature, T_{cD}^{**}, would be 1458 ± 28 K. The ratio $2\lambda/a_D$ is –759 ± 58 K. Brown et al. (1972) reported that the intensity of b-reflections from a pigeonite crystal with composition $En_{39}Fs_{52}Wo_9$ decreased with increasing temperature until they could no longer be detected at 930 ± 30 °C. Based on their structure refinement using data collected at 960 °C, Equations 13, 17, and 18 give $Q_{OD} = 0.50$. The calibration in Figure 8 gives $T_{cD}^{**} = 806$ °C for this state of

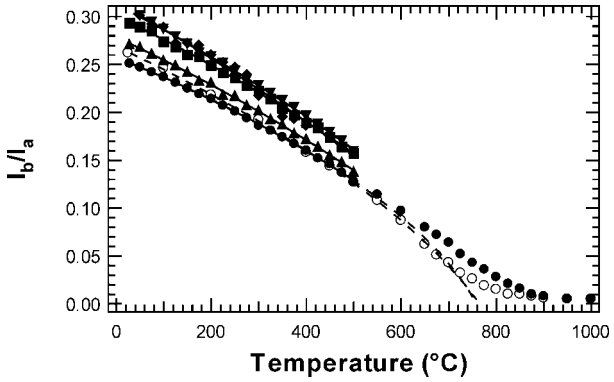

FIGURE 7. Variations of the intensity ratio $\Sigma I_b/\Sigma I_a$ as a function of temperature for pigeonite crystals BTS-308 nos. 17 and 14. The different data sets in the range up to 773 K are for crystal no. 17 before and after each ex situ heat treatment. They refer to structural states with different, fixed values of Q_{OD}. Curves through the data are fits to Equation 11. Data for crystal no. 14 are shown as filled circles (heating cycle) and open circles (cooling cycle). They show that $\Sigma I_b/\Sigma I_a$ tends to zero continuously at the phase transition. Curves through these data are also fits to Equation 11, using data up to 773 K, showing good agreement below ~900 K, but relatively poor agreement above ~950 K, where Q_{OD} changed on the timescale of the measurements.

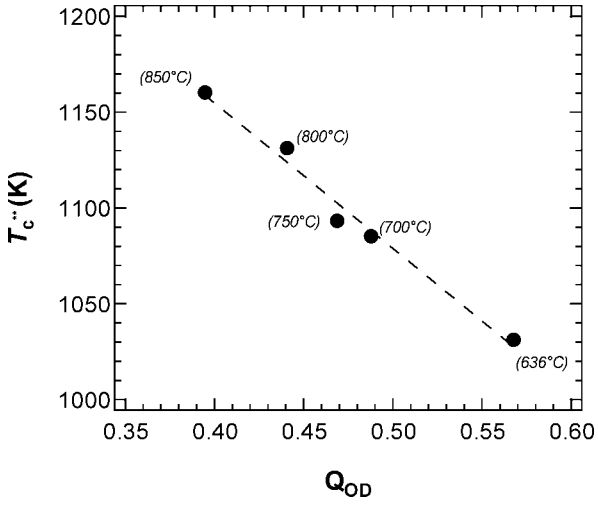

FIGURE 8. Variation of critical temperature, T_{cD}^{**}, with degree of non-convergent order, Q_{OD}, as extracted from the data for crystal no. 17 in Figure 7. The dashed line is a least-squares fit to the data: $T_{cD}^{**} = 1456(28) - 759(58)\cdot Q_{OD}$.

order, so the effect of composition must also be taken into account in predicting variations of T_{cD}^{**} for other pigeonites in the pyroxene quadrilateral.

If changes in Q_{OD} cause changes in the equilibrium variation of Q_D, it follows that changes in Q_D must cause changes in the equilibrium variation of Q_{OD}. Increasing Q_{OD} effectively suppresses Q_D and increasing Q_D should likewise act to reduce Q_{OD}. In other words, the degree of non-convergent order should be lower in the $P2_1/c$ structure than it would be in a $C2/c$ structure at the same temperature. Plots of K_D against $1/T$ should show a break in slope at the transition point for the $C2/c$-$P2_1/c$ transition and could become non-linear in the $P2_1/c$ stability field. Data for Q_{OD} as a function of temperature given above are all for crystals held within the $P2_1/c$ stability field. At 950 °C, $Q_{OD} = 0.41$ (Cámara et al. 2002) which, according to Equation 31, would fall in the stability field of the $C2/c$ structure. The data of Cámara et al. (2002) for Q_{OD} in a crystal with the same composition as used in the present study therefore span the $C2/c$-$P2_1/c$ transition. Unfortunately, only one data point is in the $C2/c$ field and it is not possible to discern a break in slope of $\ln K_D$ vs. $1/T$ (their Figure 1). On the other hand, Pasqual et al. (2000) have shown that the non-convergent ordering process in pigeonite is insensitive to bulk composition. It is known that the displacive transition is highly sensitive to composition and, in the absence of more direct evidence, it thus seems that Q_{OD} may be less sensitive to variations in Q_D. This apparent conflict between observation and prediction could be anticipated if there is a large disparity in the total energy change associated with the two processes. Phase transitions involving a classical soft mode tend to be driven by relatively small energy changes, in comparison with classical cation ordering. If this is the case for pigeonite, the effect of the Q_{OD} term in defining the equilibrium variation of Q_D in Equation 10 might be large, in comparison with the effect of the Q_D term in defining the equilibrium variation of Q_{OD} in Equation 9. Thus, the linear-quadratic coupling could have a large effect on the $C2/c$-$P2_1/c$ transition but only a small effect on the non-convergent ordering. Further experiments are required to test whether the equilibrium values of Q_{OD} are displaced enough to give detectable breaks in slope at the $C2/c$-$P2_1/c$ phase transition in plots of $\ln K_D$ against $1/T$.

According to Equation 6, the fourth order coefficient for the displacive transition, b_D^*, is expected to vary explicitly with composition but not with Q_{OD}. The experimental data for a crystal with fixed composition suggest that both the fourth and sixth order coefficients vary with Q_{OD}, however. Figure 9 shows the variations with temperature of b_D^*/a_D and c_D/a_D from Table 10. The a coefficient for a displacive phase transition is generally treated as being approximately constant for a given transition mechanism, so that the data imply decreasing b_D^* and increasing c_D with increasing Q_{OD}. If the variations are not simply an artifact of the fitting of the $\Sigma I_b/\Sigma I_a$ data over a limited temperature interval, the results suggest that b_D^* would become negative at $Q_{OD} > \sim 0.7$. In other words, the thermodynamic character of the transition can be changed from second order to first order by increasing the degree of non-convergent order. Coupling with composition, as expressed by a term such as $o_D X$ in Equation 6, may also be important in changing the sign of b_D^* from positive (second order) to negative (first order). In a crystal with composition $En_{92}Wo_8$, the transition is first order (Tribaudino et al. 2002), as it appears also to be in a crystal with composition $En_{32}Fs_{66}Wo_2$ (Smyth 1974). The conventional argument here would be that any strains which couple as $\lambda e Q^2$ can cause a change in the thermodynamic character of a phase transition, depending on the magnitude of the coupling coeffi-

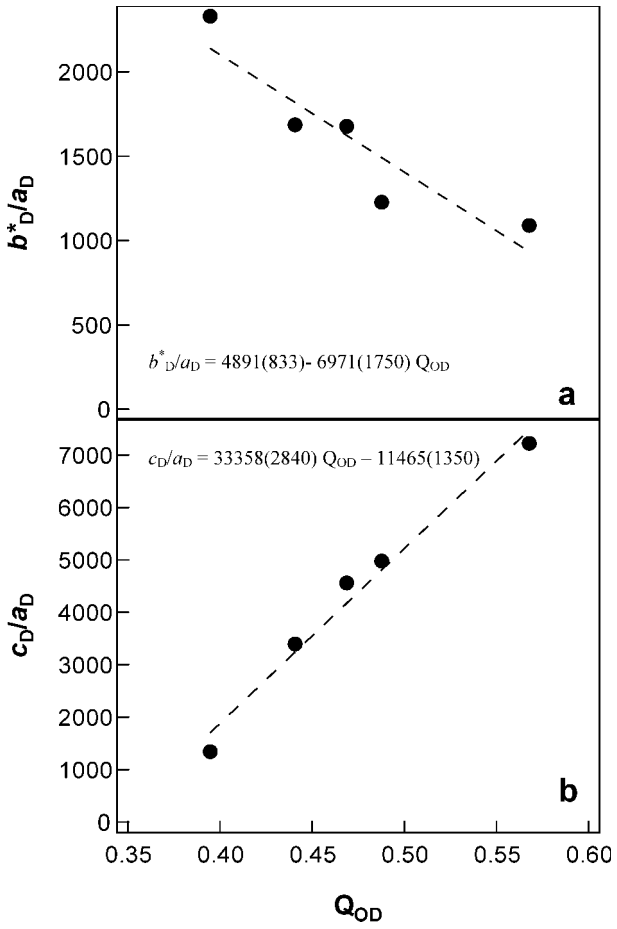

FIGURE 9. Variation of the ratios b^*_D/a_D (**a**) and c_D/a_D (**b**) with degree of non-convergent order, Q_{OD}, as extracted from the data for crystal no. 17 in Figure 7. Dashed lines are least squares fits to the data, reported in the text.

cient. Large strains may imply strong coupling and a large coupling coefficient. As seen in Equation 6, the strain coupling coefficient d_D acts to lower the value of the fourth order coefficient irrespective of its sign. There is just a hint in the data of Tribaudino et al. (2002) that this may be a factor in the dependence of the sign of b^*_D for pigeonite. Their data give a scalar strain of ~2.5% at room temperature, in comparison with ~1% for the crystal analyzed here. There are differences in the value of Q_D between these samples but the strain nevertheless seems to be significantly larger in the Fe-free sample. A significant change in the strength of coupling at different compositions could thus explain the coupling term with coefficient o_D.

In principle, the Landau expansion and experimental methodology set out above should allow the variation of transition temperature with both composition and degree of order to be defined. The qualitative result that the transition temperature decreases as the average size of the cations at the M2 site increases (Arlt et al. 2000) could then be expressed quantitatively in terms of the signs and values of the coefficients n_D and λ in Equation 8. In the model set out here, the value of λ in turn depends on the strength of coupling between each of Q_D and Q_{OD} with strain (Equation 7). For the effect of increasing Q_{OD} to be the suppression of Q_D, it follows that the strains common to both must act in opposition. From the data shown in Figure 4, this appears to be the case. The strain accompanying Q_D is opposite in sign from the strain accompanying Q_{OD} in the crystallographic **y** direction and in part of the (010) plane. This is permissive evidence in favor of the strain coupling model, but the strain data for Q_{OD} are too uncertain for definite conclusions to be drawn in this regard. Contributions to λ in the coupling term, $\lambda Q_{OD}Q_D^2$, from more direct effects of Q_{OD} on lattice vibrations (perhaps including a soft mode) cannot be ruled out.

In conclusion, the new experimental data presented here are at least consistent with a linear-quadratic coupling model for the $C2/c$-$P2_1/c$ transition. The equilibrium states of pigeonite crystals with different compositions, in terms of Q_D and Q_{OD}, are given by simultaneous solutions to Equations 9 and 10. If values of a_D and a_{OD} could be obtained from calorimetric data, it would be possible to go further and fully characterize the thermodynamic effect of the phase transition and non-convergent ordering within the pyroxene quadrilateral. Linear-quadratic coupling of this type is not commonly reported in the literature. One example is the coupling between two displacive transitions in leucite (Palmer et al. 1990; Hatch et al. 1990). For leucite, the equivalent experiment of following one order parameter in a crystal while the other is kept fixed is not possible, however, because both order parameters have a displacive origin and respond instantaneously to changes in temperature.

ACKNOWLEDGMENTS

Financial-support from the European TMR network Mineral Transformations, contract number ERB-FMRX-CT97-0108, and from Italian CNR and MURST project "Transformation, reactions, ordering in minerals," is gratefully acknowledged.

REFERENCES CITED

Angel, R.J., McCammon, C., and Woodland, A.B. (1998) Structure, ordering and cation interactions in Ca-free $P2_1/c$ clinopyroxenes. Physics and Chemistry of Minerals, 25, 249–285.

Arlt, T. and Armbruster, T. (1997) The temperature-dependent $P2_1/c - C2/c$ phase transition in the clinopyroxene kanoite $MnMg[Si_2O_6]$: a single-crystal X-ray and optical study. European Journal of Mineralogy, 9, 953–954.

Arlt, T., Kunz, M., Stolz, J., Armbruster, T., and Angel, R.J. (2000) P-T-X data on $P2_1/c$-clinopyroxenes and their displacive phase transitions. Contributions to Mineralogy and Petrology, 138, 35–45.

Blessing, R.H., Coppens, P., and Becker, P. (1974) Computer analysis of step scanned X-ray data. Journal of Applied Crystallography, 7, 488–492.

Brown, G.E., Prewitt, C.T., Papike, J.J., and Sueno, S. (1972) A comparison of the structures of low and high pigeonite. Journal of Geophysical Research, 77, 5778–5789.

Cámara, F., Carpenter, M.A., Domeneghetti, M.C., and Tazzoli, V. (2002) Non-convergent ordering and displacive phase transition in pigeonite: in-situ HT XRD study. Physics and Chemistry of Minerals, 29, 331–340.

Cámara, F., Iezzi, G., and Oberti, R. (2003) HT-XRD study of synthetic ferrian magnesian spodumene: the effect of site dimension on the $P2_1/c - C2/c$ phase transition. Physics and Chemistry of Minerals, 30, 20–30.

Cannillo, E., Germani, G., and Mazzi, F. (1983) New crystallographic software for Philips PW 1100 single crystal diffractometer. CNR Centro di Studio per la Cristallografia, Internal Report 2.

Carpenter, M.A. (1992) Thermodynamics of phase transitions in minerals: a macroscopic approach. In G.D. Price and N.L. Ross Eds., The stability of minerals, p 172–215. Chapman and Hall, London.

Carpenter, M.A. and Salje, E.K.H. (1994) Thermodynamics of nonconvergent cation ordering in minerals: II. Spinels and the orthopyroxene solid solution. American Mineralogist, 79, 1068–1083.

Carpenter, M.A., Powell, R., and Salje, E.K.H. (1994) Thermodynamics of nonconvergent cation ordering in minerals: I. An alternative approach. American Mineralogist, 79, 1053–1067.

Carpenter, M.A., Salje, E.K.H., and Graeme-Barber, A. (1998) Spontaneous strain as a determinant of thermodynamic properties for phase transitions in minerals. European Journal of Mineralogy, 10, 621–691.

Hahn, T. Ed. (1995) International Tables for Crystallography, vol. A. Kluwer Academic Publishers, Dordrecht, The Netherlands.

Hatch, D.M., Ghose, S., and Stokes, H.T. (1990) Phase transitions in leucite, $KAlSi_2O_6$ I. Symmetry analysis with order parameter treatment and the resulting microscopic distortions. Physics and Chemistry of Minerals, 17, 220–227.

Hawthorne, F.C., Ungaretti, L., and Oberti, R. (1995) Site populations in minerals: terminology and presentation of results of crystal-structure refinement. Canadian Mineralogist, 33, 907–911.

Lehmann, M.S. and Larsen, F.K. (1974) A method for location of the peaks in step-scan-measured Bragg reflections. Acta Crystallographica, A30, 580–584.

North, A.C.T., Phillips, D.C., and Mathews, F.S. (1968) A semi-empirical method of absorption correction. Acta Crystallographica, A24, 351–359.

Palmer, D.C., Bismayer, U., and Salje, E.K.H. (1990) Phase transitions in leucite: order parameter behaviour and the Landau potential deduced from Raman spectroscopy and birefringence studies. Physics and Chemistry of Minerals, 17, 259–265.

Pannhorst, W. (1984) High temperature crystal structure refinements of low-clinoenstatite up to 700°C. Neues Jahrbuch für Mineralogie Abhandlungen, 150, 219–228.

Pasqual, D., Molin, G., and Tribaudino, M. (2000) Single-crystal thermometric calibration of Fe-Mg order-disorder in pigeonites. American Mineralogist, 85, 953–962.

Prewitt, C.T., Brown, G.E., and Papike, J.J. (1971) Apollo 12 clinopyroxenes: high temperature X-ray diffraction studies. Proceedings of the Second Lunar Science Conference, 1, 59–68. M.I.T. Press.

Salje, E.K.H. (1985) Thermodynamics of sodium feldspar I: order parameter treatment and strain induced coupling effects. Physics and Chemistry of Minerals, 12, 93–98.

Salje, E.K.H. and Kroll, H. (1991) Kinetic rate laws derived from order parameter theory: III. Al, Si ordering in sanidine. Physics and Chemistry of Minerals, 17, 563–568.

Salje, E.K.H., Kuscholke, B., Wruck, B., and Kroll, H. (1985) Thermodynamics of sodium feldspar II: experimental results and numerical calculations. Physics and Chemistry of Minerals, 12, 99–107.

Schröpfer, L. (1985) Observation of reactions in Synthetic Ca-poor pyroxene single crystals at elevated temperatures by X-ray diffraction. Physics and Chemistry of Minerals, 12, 49–54.

Sheldrick, G.M. (1997) SHELX-97, program for crystal structure determination. University of Göttingen, Germany.

Smyth, J.R. (1974) The high temperature crystal chemistry of clinohypersthene. American Mineralogist, 59, 1069–1082.

Tribaudino, M. (2000) A transmission electron microscope investigation of the $C2/c \rightarrow P2_1/c$ phase transition in clinopyroxenes along the diopside-enstatite ($CaMgSi_2O_6$–$Mg_2Si_2O_6$) join. American Mineralogist, 85, 707–715.

Tribaudino, M., Nestola, F., Cámara, F., and Domeneghetti, M.C. (2002) The high-temperature $P2_1/c \rightarrow C2/c$ phase transition in Fe-free pyroxene ($Ca_{0.15}Mg_{1.85}Si_2O_6$): structural and thermodynamic behavior. American Mineralogist, 87, 648–657.

Wilson, A.J.C. Ed. (1995) International Tables for Crystallography, vol. C. Kluwer Academic Publishers, Dordrecht, The Netherlands.

Woodland, A.B., McCammon, C., and Angel, R.J. (1997) Intersite partitioning of Fe and Mg in Ca-free high-pressure $C2/c$ clinopyroxene. American Mineralogist, 82, 923–930.

Zema, M., Domeneghetti, M.C., Molin, G.M., and Tazzoli, V. (1997) Cooling rates of diogenites: a study of Fe^{2+}-Mg ordering in orthopyroxene by single-crystal X-ray diffraction. Meteoritics and Planetary Science, 32, 855–862.

Zhang, M., Redhammer, G.J., Salje, E.K.H., and Mookherjee, M. (2002) $LiFeSi_2O_6$ and $NaFeSi_2O_6$ at low temperatures: an infrared spectroscopic study. Physics and Chemistry of Minerals, 29, 609–616.

MANUSCRIPT RECEIVED MAY 31, 2002
MANUSCRIPT ACCEPTED FEBRUARY 24, 2003
MANUSCRIPT HANDLED BY DONALD ISAAK